

## Antibacterial, optical, and microstructural properties investigations of Ag-doped TiO<sub>2</sub> and TiO<sub>2</sub>/PVA nanocomposite powders

*Ag katkılı TiO<sub>2</sub> ve TiO<sub>2</sub>/PVA nanokompozit tozların antibakteriyel, optik ve mikroyapısal özelliklerinin araştırılması*

Şeyma DUMAN<sup>\*1,a</sup>, Büşra BULUT<sup>1,b</sup>

<sup>1</sup> Bursa Technical University, Engineering and Natural Sciences Faculty, Metallurgical and Materials Engineering Department, 16310, Bursa

• Geliş tarihi / Received: 10.10.2021

• Düzeltilek geliş tarihi / Received in revised form: 16.03.2022

• Kabul tarihi / Accepted: 26.03.2022

### Abstract

This research aims to investigate the microstructural, optical, and antibacterial properties of silver (Ag) doped titanium dioxide (TiO<sub>2</sub>) and titanium dioxide - polyvinyl alcohol (TiO<sub>2</sub>/PVA) nanocomposite powders synthesized by the sol-gel method. The powder state characterization of the nanocomposite powders was performed with SEM, EDS, XRD, laser particle size, specific surface area, density measurements, UV-vis analysis, and antibacterial tests. SEM examinations demonstrated that titanium dioxide nanoparticles synthesized using PVA dopant have relatively spherical morphology. It detected that pure, Ag-doped TiO<sub>2</sub> and Ag-doped TiO<sub>2</sub>/PVA nanocomposite powders are in an anatase phase by XRD microanalysis. The existence of silver in the nanocomposite powders was detected by EDS analysis, XRD, and UV-vis in peak shifts. The silver and polymer dopings were decreased surface area and density values for the TiO<sub>2</sub> system. The addition of Ag to the nanocomposite powders significantly improved the antibacterial properties of the synthesized TiO<sub>2</sub> and TiO<sub>2</sub>/PVA nanocomposite powders against Staphylococcus aureus (S. aureus) and Escherichia coli (E. coli). However, it determined that the antibacterial activity effect was little on E. coli compared to S. aureus.

**Keywords:** Ag, Antibacterial properties, Microstructural properties, Optical properties, PVA, TiO<sub>2</sub>

### Öz

*Bu çalışmanın amacı, sol-jel prosesi ile sentezlenen gümüş (Ag) katkılı titanyum dioksit (TiO<sub>2</sub>) ve titanyum dioksit - polivinil alkol (TiO<sub>2</sub>/PVA) nanokompozit tozların mikroyapısal, optik ve antibakteriyel özelliklerini araştırmaktır. Nanokompozit tozların toz karakterizasyonu, SEM, EDS, XRD, lazer partikül boyutu, spesifik yüzey alanı, UV-vis analizi ve yoğunluk ölçümleri ile gerçekleştirilmiştir. SEM incelemeleri, PVA katkı maddesi kullanılarak sentezlenen TiO<sub>2</sub> nanopartiküllerin nispeten küresel morfolojiye sahip olduğunu gösterdi. Katkısız ve Ag katkılı TiO<sub>2</sub>/PVA nanokompozit tozların XRD mikroanalizi ile anataz fazında olduğu tespit edildi. Nanokompozit tozlarda gümüşün varlığı, EDS analizi, XRD ve UV-vis pik kaymaları ile tespit edildi. Gümüş ve polimer katkılama, TiO<sub>2</sub> sisteminde yüzey alanı ve yoğunluk değerlerini azaltmıştır. Nanokompozit tozlara Ag katkulanırılması, sentezlenen TiO<sub>2</sub> ve TiO<sub>2</sub>/PVA nanokompozit tozların Staphylococcus aureus (S. aureus) ve Escherichia coli (E. coli)'ye karşı antibakteriyel aktivitesini önemli ölçüde iyileştirmiştir. Ayrıca, antibakteriyel aktivite etkisinin S. aureus'a kıyasla E. Coli üzerine daha az olduğu saptanmıştır.*

**Anahtar kelimeler:** Ag, Antibakteriyel özellikler, Mikroyapısal özellikler, Optik özellikler, PVA, TiO<sub>2</sub>

<sup>\*a</sup> Şeyma DUMAN; seyma.duman@btu.edu.tr, Tel: (0224) 300 37 34, orcid.org/0000-0002-6685-5656

<sup>b</sup> orcid.org/0000-0002-9946-6729

## 1. Introduction

### 1. Giriş

Among various metal oxides, TiO<sub>2</sub> nanoparticles have been the focus of researchers resulting from their biocompatibility, non-toxicity, chemical and physical stability, photocatalytic and antibacterial activity (Seery et al., 2007; Zhang et al., 2012; Bahadur et al., 2016). These unique properties have been prevalently studied in literature for the removal of harmful bacteria or organic and inorganic pollutants in wastewater or air and for self-sterilizing surfaces (Seery et al., 2007; Mogal et al., 2014). Moreover, it has been stated that the anatase form of TiO<sub>2</sub> possesses excellent antibacterial behavior under the illumination of UV light (Jamuna-Thevi et al., 2011; Bahadur et al., 2016). However, the disadvantages of TiO<sub>2</sub> with its wide bandgap (about 3.2 eV), such as absorbing UV light, which is a small part of the solar spectrum (<5 %), and exhibiting only antibacterial properties under the UV light, limits its wide applications (Seery et al., 2007; Zhang et al., 2012; Li et al., 2018). Accordingly, numerous studies have been accomplished to enhance the visible light activity by doping TiO<sub>2</sub> with transition metals (Chao et al., 2003; Seery et al., 2007; Bahadur et al., 2016; Li et al., 2018; Viet et al., 2018). Among them, silver (Ag) nanoparticles are one of the most widely used transition metals that extend the absorption capability in the visible region (Li et al., 2018). Furthermore, Ag nanoparticles have a strong antibacterial, antiviruses, and antifungal activity against many kinds of bacteria (Kawashita et al., 2000; Cheng et al., 2006; Sun et al., 2008; Bahadur et al., 2016). Feng et al., (2000) reported that Ag induced the inactivation of bacterial proteins in their study examining the antibacterial effect of Ag on bacteria. Hence, incorporation of Ag into TiO<sub>2</sub> composites is expected to exhibit higher antibacterial properties than the pure TiO<sub>2</sub> (Behnajady et al., 2008) and to be potential candidate for antibacterial materials (Bahadur et al., 2016).

There are various methods such as chemical reduction, mechanochemical technique, co-precipitation method, hydrothermal method, and sol-gel method to synthesis nanoparticles (Yin et al., 2003; Wang, 2007; Lee et al., 2016; Abbad et al., 2020; Bulut & Duman, 2021). Among the above-stated methods, the sol-gel method is the most common preferred method for Ag-doped TiO<sub>2</sub> nanoparticle synthesis. This method is the simplest method having advantages, such as a higher purity, a better homogeneity, a lower cost, a lower processing temperature, and the ability to go

from molecular precursor to the product (Brinker et al., 1991; Wang et al., 1999; Feng et al., 2005; Mathews et al., 2009; Haque et al., 2017). Recently, the synthesis of nanoparticles grew in importance due to enhanced surface area/volume ratio, modification of structure, and enhanced activity by comparison with micron sizes of particles. Because of the Van der Waals forces between nanoparticles, agglomeration generates. Therefore, nanoparticle-coating is significant that the Van der Waals forces between nanoparticles reduced, and the distribution of nanoparticles in the composite increased. Polymers such as polyethylene glycol (PEG), polyvinyl chloride (PVC), polyvinyl pyrrolidone (PVP), polyvinyl alcohol (PVA) are commonly preferred in nanoparticle coating (Chang et al., 2003; Shenhar et al., 2005; Guo et al., 2006; Han & Yu., 2006; Wu & Ke., 2007; Chandra et al., 2008). PVA has wide application in the biomedical field due to these features, such as non-toxic, non-carcinogenic, high hydrophilicity, biocompatibility, and biodegradability (Francis et al., 2004; Bandyopadhyay et al., 2005; Varshney, 2007). These properties allow usage of PVA for different medical applications such as drug coating agents, cosmetic industries, surgical sutures materials (Crispim et al., 2012; Swaroop et al., 2016). PVA possesses poor antibacterial ability (Fang et al., 2019). However, doping PVA to silver nanoparticles could enhance antibacterial activity, which is highly coveted in biomedical area. The inclusion of silver nanoparticles in the PVA polymer matrix could provide antibacterial activity, which is highly desirable in the medical field by killing the bacteria on site (Swaroop et al., 2016).

This work aimed to investigate the morphology and the antibacterial properties of pure, Ag-doped TiO<sub>2</sub> and TiO<sub>2</sub>/PVA nanocomposite powders synthesized by the sol-gel method. The influences of Ag dopant concentration and PVA coating of particles on the nanocomposite powders were examined. The characterization of the nanocomposite powders was carried out using scanning electron microscopy (SEM), X-ray fluorescence spectroscopy (XRF), energy dispersive spectroscopy (EDS), X-ray diffraction (XRD), laser particle size (LPS), specific surface area, UV-visible spectrophotometer, Arnold apparent and helium pycnometer density measurements. The antibacterial behavior of the nanocomposite powders was analysed. The results displayed that the joining of Ag can significantly enhance the antibacterial behavior of the produced

nanocomposite powders by developing their optical properties.

## 2. Material and methods

### 2. Malzeme ve yöntemler

#### 2.1. Raw materials and powder synthesis

##### 2.1. Hammaddeler ve toz sentezi

Titanium (IV) isopropoxide (TTIP) and urea were used, which were purchased from Sigma Aldrich™ (USA). Silver nitrate ( $\text{AgNO}_3$ , Alfa Aesar™, 99.9% purity) and polyvinyl alcohol (PVA, Merck™, MW=72,000 g/mol) were selected as dopant material and binder, respectively. Moreover, distilled water and ethanol (Sigma Aldrich™) were used in the experiments. 1 mol of TTIP was put in a 50 ml beaker consisting of 10 ml ethanol and 35 ml distilled water. The solution was stirred for 10 minutes to adjust the pH to 2.5 using a pH meter and afterward continued to mix at 50 minutes by adding 1 mol hydrochloric acid (HCl) drop-by-drop until the pH to 1. A homogeneous

clear yellow solution identified as the solution-A was obtained. 3 wt. % of PVA was solved in 10 ml of distilled water and obtained a solution coded as B was loaded dropwise to solution-A and mixed for an hour. 5 ml of distilled water and 2 or 4 wt. % of  $\text{AgNO}_3$  were mixed for 5 minutes and thus, solution-C was prepared. Solution-C was loaded dropwise to solution-A and stirred for half-hour. The prepared solution waited at room temperature for 2 hours and a gel was obtained by drying oven at 110 °C for 6 hours, and obtained powder was grinded. Finally, calcination experiment of dried powders was realized in a muffle-type furnace at 450 °C for 2 hours.

The sample codes of compositions of the nanocomposite powders are given in Table 1.  $\text{TiO}_2$  nanoparticles,  $\text{AgNO}_3$ , and PVA, which are coded to as T, A, and P, were used in the experimental study. The synthesis of the Ag-doped  $\text{TiO}_2$  and  $\text{TiO}_2$ /PVA nanocomposite powders is schematically represented in Figure 1.

**Table 1.** The samples codes and compositions.

**Tablo 1.** Numune kodları ve kompozisyonlar.

Final Sample codes	Composition of the solutions		$\text{AgNO}_3$ , wt. %	PVA, wt. %
	Initial sample content			
T	TTIP		-	-
T-2A	TTIP - 2 wt. % $\text{AgNO}_3$		2	-
T-2A3P	TTIP - 2 wt. % $\text{AgNO}_3$ - 3 wt. % PVA		2	3
T-4A	TTIP - 4 wt. % $\text{AgNO}_3$		4	-
T-4A3P	TTIP - 4 wt. % $\text{AgNO}_3$ - 3 wt. % PVA		4	3

#### 2.2. Characterization procedures

##### 2.2. Karakterizasyon prosedürleri

SEM (FESEM, Carl Zeiss™ Gemini 300, Germany) and EDS characterized the morphology of the synthesized Ag-doped  $\text{TiO}_2$  and  $\text{TiO}_2$ /PVA nanocomposite powders. The obtained samples were covered with an admixture of gold and palladium layers before their SEM examination operated at 15 kV. Crystalline phases of the Ag-doped  $\text{TiO}_2$  and  $\text{TiO}_2$ /PVA nanocomposite powders were identified using a Bruker™ AXS/Discovery D8 XRD connected with Lynxeye XE detector with  $\text{CuK}\alpha$  (1.54060 Å) radiation. XRD patterns were recorded operating at 40 kV and 40 mA over an angular range of 20 to 70° with a step size of 0.05° per step. The obtained XRD patterns were matched to crystalline phases from

the PDF 4-2016 Powder Diffraction database of the International Centre for Diffraction Data (ICDD).

Particle size measurements of nanocomposite powders were conducted using a Malvern™ Mastersizer 3000 particle size analyzer. The specific surface area of the prepared nanocomposite powders was determined by the Brunauer–Emmett–Teller (BET) method via Micromeritics™ Tristar II 3020 analyzer. For this purpose, all samples were outgassed for at least 3 h at 120 °C before the adsorption measurements. The apparent and pycnometer densities of nanocomposite powders were mensurated with Arnold density measurement kit and helium pycnometer (Micromeritics™, Accupyc 1330), respectively. The optical absorbance of synthesized Ag-doped  $\text{TiO}_2$  and  $\text{TiO}_2$ /PVA nanocomposite powders was determined by a UV–vis

spectrophotometer (Agilent™ – Cary60) in the wavelength range between 200 and 800 nm.

Antibacterial activity analysis was carried out according to the ASTM 2149 method. Staphylococcus aureus (S. aureus), yeast, and mold ATCC 6538 and ATCC) were used as micro-organism suspensions. These suspensions were tested with Model bacteria Escherichia coli (E. coli) at pH 7 in Maximum Recovery Diluent with different nanocomposite powders. This process was briefly performed as follows: Nanocomposite powders weighing 1g were put in a 250 ml flask containing 50 ml of microorganism solution. The certain flasks were quivered at 37 °C in an incubator, and dispersion samples were gathered after ten minutes, 20 minutes, and 30 minutes of contact times. Diluted solutions touching the surfaces were set on Muller-Hinton II agar and incubated for 24 h at 37 °C. Moreover, colony counts were made to assign the existence of viable bacteria.

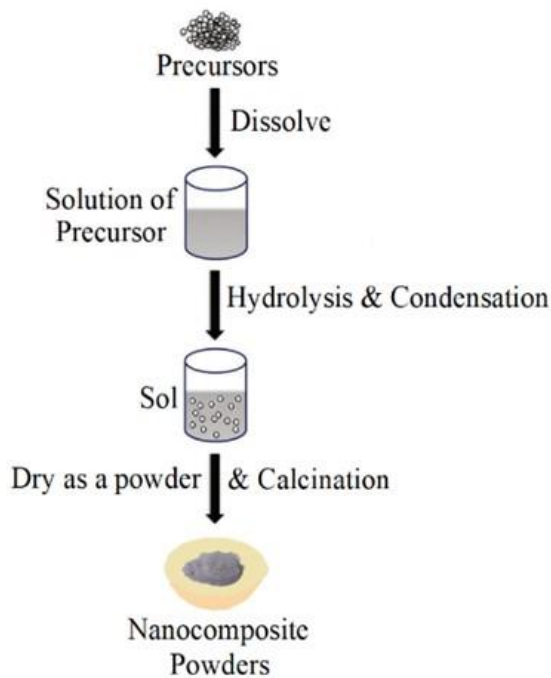


**Figure 1.** Schematics diagrams of synthesis of the Ag-doped TiO<sub>2</sub> and TiO<sub>2</sub>/PVA nanocomposite powders.

**Şekil 1.** Ag katkılı TiO<sub>2</sub> ve TiO<sub>2</sub>/PVA nanokompozit tozlarının sentezinin şematik diyagramları.

### 3. Results and discussion

#### 3. Bulgular ve tartışma

One of the significant parameters in sol-gel is the hydrolysis ratio affecting the viscosity, gelation time, and structure of the product. A lower amount of water is required to form a low crosslinking of the product and a high sol viscosity. However, the higher amount of water causes the highly crosslinking product and the low sol viscosity (Liu & Shaw., 2015; Ye, 2018). Therefore, the first step in sol-gel experiments is to determine the optimal hydrolysis ratio. It was observed that the pH in sol-gel parameters affected the particle size of the end-product. The obtained results in the literature demonstrated that the pH value and hydrolysis ratio have a synergistic effect on the microstructures of the products (Lee et al., 2016; Ye, 2018). Sol-gel reactions can be catalyzed by both acids and bases. Another parameter is reaction temperature influencing both hydrolysis and condensation rate (Livage et al., 1988; Liu & Shaw., 2015). In our sol-gel experiments, optimal values of pH, catalyst, drying temperature, and calcination temperature were selected at 1, HCl, 110 °C, and 450 °C, respectively.

#### 3.1. Microstructural properties of nanocomposite powders

##### 3.1. Nanokompozit tozların mikroyapısal özellikleri

It is usually desired that the powders be in spherical morphology for improving physical properties like flowability, bulk density, and product appearance. To achieve spherical morphology during sol-gel, TiO<sub>2</sub> and Ag-doped TiO<sub>2</sub> sols must disperse in the form of an emulsion by using an organic solvent (Aksu et al., 2020). The binder was added into the sol for the production of spherical particles and then dried. Herein, PVA was selected as the binder. The effects of the PVA on the morphology of starting materials after sol-gel were examined using SEM in Figure 2. As shown in Figures 2a, 2b, and 2d, spherical morphology was not visible in the samples without PVA dopant. The AgNO<sub>3</sub> doped nanocomposite powders led to the formation of spherical granule shapes (Figures 2b, 2c, 2d, and 2e). As seen in the SEM micrographs, PVA is an appropriate binder for ensuring more stable spherical particles (Jr Walker et al., 1999). On the other hand, the spherical powders of T-2A3P and T-4A3P nanocomposite powders indicate smoother surface shape and denser structure (Figure 2).

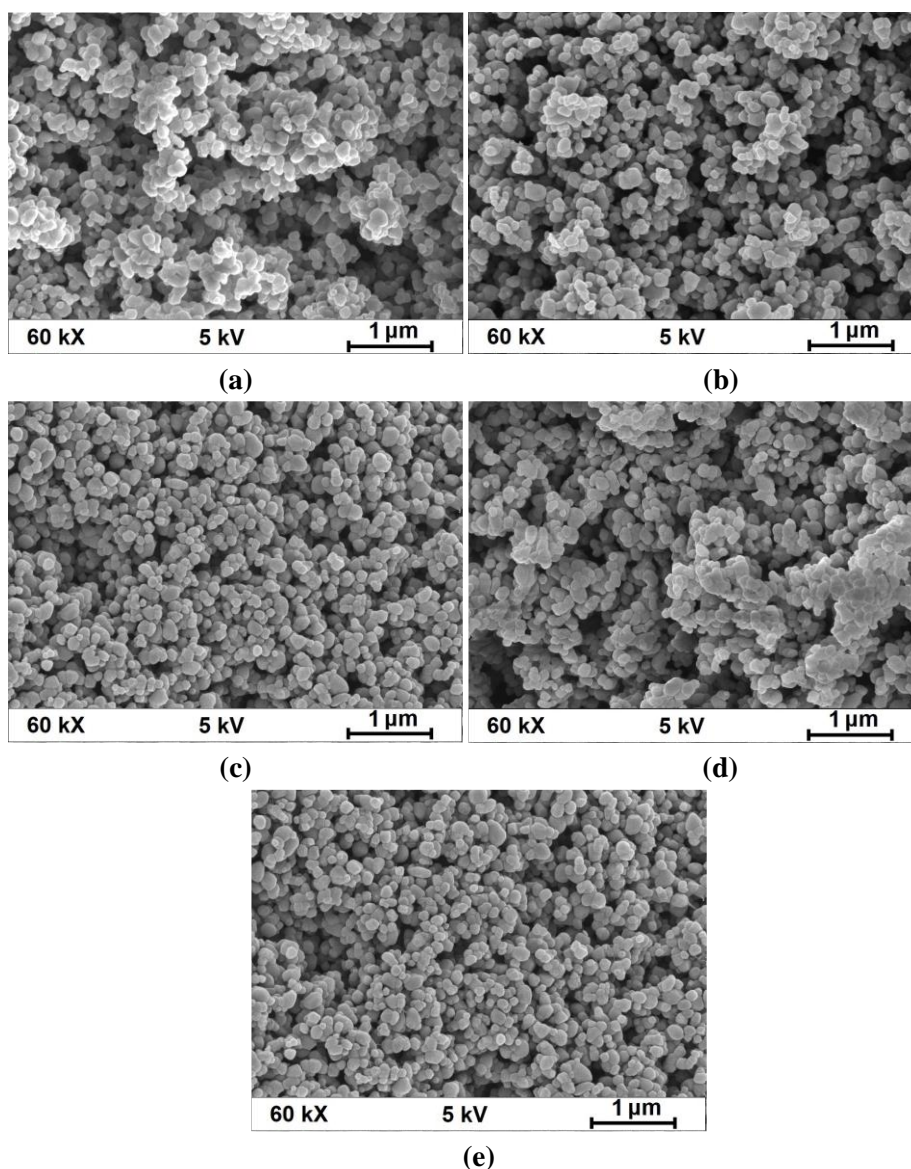


**Figure 2.** SEM images of initial and synthesized nanocomposite powders: (a) T, (b) T-2A, (c) T-2A3P, (d) T-4A, and (e) T-4A3P.

**Şekil 2.** Başlangıç ve sentezlenmiş nanokompozit tozların SEM görüntüleri: (a) T, (b) T-2A, (c) T-2A3P, (d) T-4A ve (e) T-4A3P.

The XRF results are given in Table 2. The XRF outcome validated the successful doping of Ag into the synthesized  $\text{AgNO}_3$  doped  $\text{TiO}_2/\text{PVA}$ . For 2 % and 4 %  $\text{AgNO}_3$  actual Ag transfer were determined as 0.49% and 2.3%, respectively, for  $\text{TiO}_2$  system. Besides, the percent of Ag of T-2A3P and T-4A3P samples was 1.1% and 2.8% for  $\text{TiO}_2/\text{PVA}$  system. It has shown that Ag ions have entered the lattices of  $\text{TiO}_2$ . As noted above, it is come out that the existence of silver is determined from XRD peak shift and XRF elemental analysis in both  $\text{TiO}_2$  system.

Particle sizes and the surface areas distribution of  $\text{TiO}_2$  system are given in Table 1. The particle size measurements for  $\text{TiO}_2$  systems range between 310.2 and 259.9 nm. In both  $\text{TiO}_2$  and  $\text{TiO}_2/\text{PVA}$

nanocomposite powders, a decrease in particle size due to granulation was observed. It was found that the BET surface area is 11.12 and 9.46  $\text{m}^2/\text{g}$  for the starting  $\text{TiO}_2$  material and the T-4A3P product, respectively. On the other hand, a decrease in BET values was observed for  $\text{TiO}_2$  based systems due to spherical morphology.

Apparent and pycnometer densities of the initial and the nanocomposite powders are given in Table 2. An increase was observed due to the addition of PVA for the apparent density values of  $\text{TiO}_2/\text{PVA}$  nanocomposite powders. It was stated in the previous studies (Duman & Özkal., 2012) that packaging behaviours of nanopowders synthesized sol-gel method enhanced. The theoretical density for  $\text{TiO}_2$  was at 4.23  $\text{g}/\text{cm}^3$ , and a value (4.18

g/cm<sup>3</sup>) close to this value was obtained by pycnometer density measurement. It was observed that the pycnometer densities increase with the addition of Ag while they decrease with the addition of binder in TiO<sub>2</sub> and TiO<sub>2</sub>/PVA nanocomposite powders.

Figure 3. shows the XRD patterns of the TiO<sub>2</sub> and TiO<sub>2</sub>/PVA nanocomposite powders. Both the powders synthesized by the sol-gel method have tetragonal structure, and their XRD peaks were in good agreement with the JCPDS card no. 78-2486 for TiO<sub>2</sub> (Figure 3).

**Table 2.** Percentages of Ag, particle sizes and specific surface areas values of both in TiO<sub>2</sub> system.

**Tablo 2.** Her iki TiO<sub>2</sub> sisteminin Ag yüzdeleri, partikül boyutları ve spesifik yüzey alanı değerleri.

Sample code	Percent of Ag (wt.%)	Particle size (nm)	Surface Area-BET (m <sup>2</sup> /g)	Apparent Density (g/cm <sup>3</sup> )	True Density (g/cm <sup>3</sup> )	Theoretical Density (g/cm <sup>3</sup> )
T	-	306	11.12	0.34 ±0.04	4.18	4.23
T-2A	0.49	310.2	10.99	0.41±0.04	4.32	4.36
T-2A3P	1.1	303.7	9.60	0.39 ±0.03	4.23	4.26
T-4A	2.3	277.1	10.01	0.46±0.05	4.44	4.48
T-4A3P	2.8	259.9	9.46	0.41 ±0.03	4.34	4.39

In Figure 3a, the diffraction peaks at 2-theta of 25.3°, 37.8°, 48.0°, 53.9°, 55.1°, 62.7°, and 75.1° are ascribed to (101), (004), (200), (105), (211), (204), and (215) planes of TiO<sub>2</sub>. TiO<sub>2</sub> crystals have lattice parameters of a = 3.78 Å and c = 9.51 Å. The nanocomposite powders show that the synthesized nanoparticles in this research have the anatase phase. There are no additional peaks beyond the anatase phase for Ag-doped TiO<sub>2</sub> nanocomposite powders, respectively. Figure 3(c) and 3(d) show enlarged views of the (101) peak (in the 2θ range of 24-27°) in the TiO<sub>2</sub> nanocomposite powders. Herein, shifts in the peak were observed in the TiO<sub>2</sub>-based-system.

The average crystallite size has been computed from the highest intensity peak of the synthesized Ag-doped TiO<sub>2</sub> and TiO<sub>2</sub>/PVA nanocomposite powders with the help of XRD peak broadening estimation by the Debye-Scherrer's equation as follows:

$$D = \frac{k\lambda}{\beta \cos \theta} \tag{1}$$

where 'D' is the crystallite size, k is the shape factor of value 0.9, 'λ' is the X-ray wavelength (1.54 Å), 'θ' and 'β' are Bragg's angle and full width at half maximum (FWHM) of a predictive peak respectively (Holzwarth & Gibson., 2011). The lattice strain of all synthesized nanoparticles was counted using The Williamson-Hall (W-H) method (Williamson & Hall., 1953). The W-H graph is procured using the following equation:

$$\beta \cos \theta = 4\epsilon \sin \theta + (0.90\lambda / \beta \cos \theta) \tag{2}$$

where 'ε' is the lattice strain presents in the synthesized Ag-doped TiO<sub>2</sub> and TiO<sub>2</sub>/PVA nanocomposite powders. The lattice strain is assessed from the slope of a plot of βCosθ versus 4sinθ. The crystallite size of the synthesized undoped and Ag-doped TiO<sub>2</sub> and TiO<sub>2</sub>/PVA nanocomposite powders by the sol-gel method are estimated and seen in Table 3. As it can be seen from Table 3, the crystallite size decreases as the 2θ value increases.

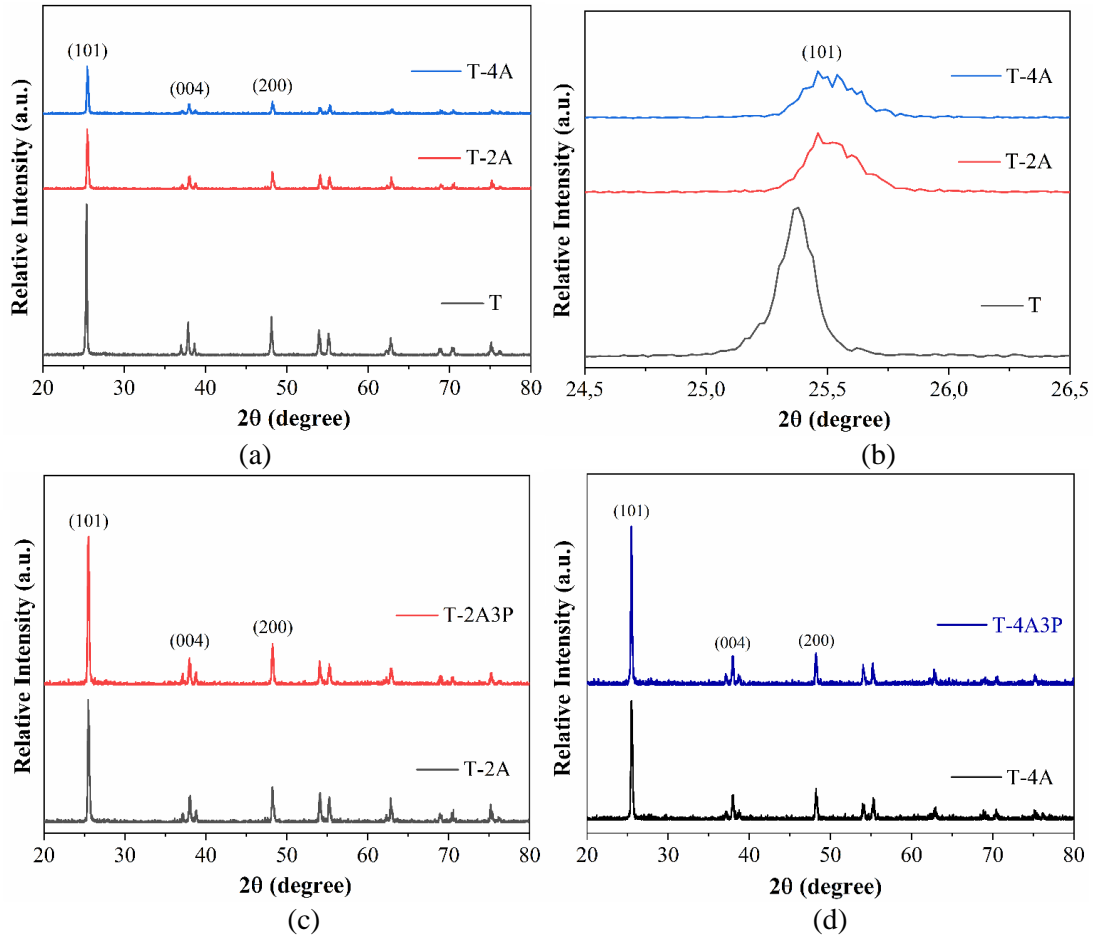


**Figure 3.** XRD patterns of initial and the synthesized nanocomposite powders.  
**Şekil 3.** Başlangıç ve sentezlenmiş nanokompozit tozların XRD paternleri.

**Table 3.** Geometric parameters of the synthesized Ag-doped TiO<sub>2</sub> and TiO<sub>2</sub>/PVA nanocomposite powders.

**Tablo 3.** Sentezlenen Ag katkılı TiO<sub>2</sub> ve TiO<sub>2</sub>/PVA nanokompozit tozların geometrik parametreleri.

Sample code	2θ°	hkl	Crystallite size (nm)
T	25.39	(101)	29.2 ± 0.3
T-2A	25.61	(101)	25.7 ± 0.5
T-2A3P	25.63	(101)	20.8 ± 0.2
T-4A	25.67	(101)	20.1 ± 0.3
T-4A3P	26.35	(101)	14.4 ± 0.2

### 3.2. Optical properties of nanocomposite powders

#### 3.2. Nanokompozit tozların optik özellikleri

Effect of Ag on optical properties of the synthesized TiO<sub>2</sub> and TiO<sub>2</sub>/PVA nanocomposite powders by sol-gel method were detected using UV-vis Spectrometer analysis at room temperature. The optical absorption spectra of pure and Ag-

doped TiO<sub>2</sub> and TiO<sub>2</sub>/PVA nanocomposite powders are given in Figure 4. These absorption spectra indicated a redshift of the light absorption edge of Ag-doped TiO<sub>2</sub> and TiO<sub>2</sub>/PVA nanocomposite powders. The level of redshift has increased with increasing the amounts of Ag. On the other hand, Ag doping causes a reduction in bandgap energy due to the redshift of light absorption. The shifting of the light absorption

edge of TiO<sub>2</sub> nanopowders after transition metal ion doping was also reported in other studies (Ahamed et al., 2017; Ali et al., 2018; Yildirim, 2021).

Tauc Model was used to specify the optical bandgap energy of the nanocomposite powders, according to the following equation (Ahamed et al., 2016; Ahamed et al., 2017):

$$\alpha h\nu = A (h\nu - E_g)^m \quad (3)$$

where ‘ $\alpha$ ’ is the absorption coefficient, ‘ $h\nu$ ’ is the photon energy, ‘ $A$ ’ is an energy-independent constant, ‘ $E_g$ ’ is the optical bandgap, and ‘ $m$ ’ is

equal to 1/2 for allowed direct optical transitions. Herein, the optical bandgap energy can determine by performing Equation (3) to the UV–VIS spectra of the nanocomposite powders. The direct band gap values were determined corresponding to 3.34 eV, 3.27 eV, 3.26 eV, 3.18 eV, and 3.17 eV for T, T-2A, T-2A3P, T-4A, and T-4A3P, respectively (Table 4). It was determined that bandgap energy ( $E_g$ ) of TiO<sub>2</sub> nanopowders decreases from 3.34 eV to 3.17 eV when increasing the concentration of Ag dopant. Decreasing band gap energy of TiO<sub>2</sub> nanopowders after doping with metal ions is also reported by other researchers (Zhang et al., 2014; Santos et al., 2015; Ahamed et al., 2017).

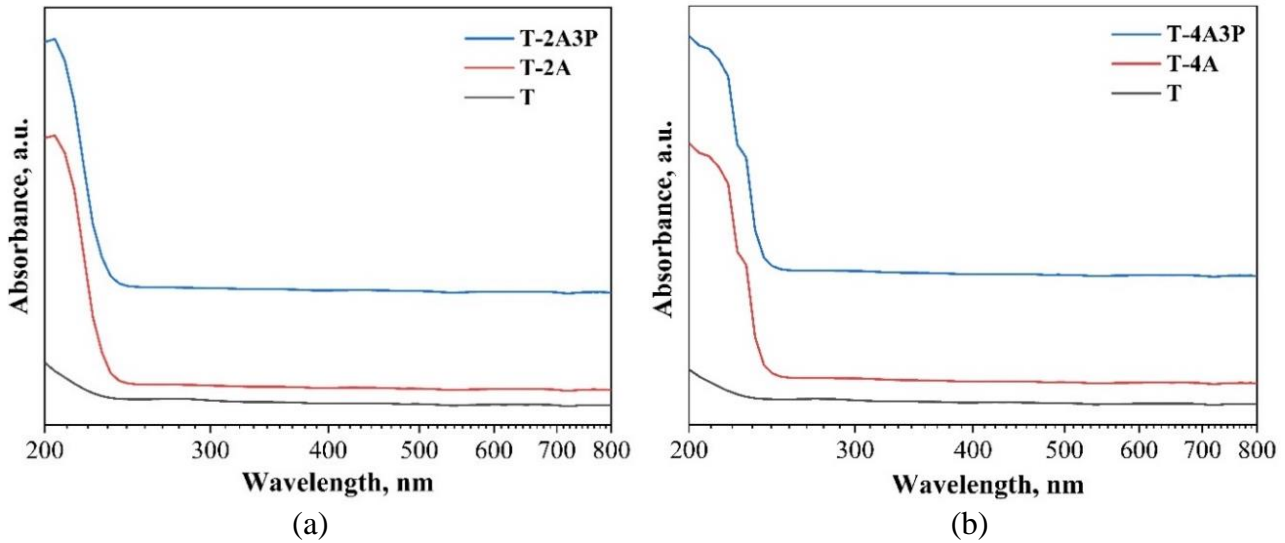


**Figure 4.** UV-vis peaking values of the synthesized nanocomposite powders by sol-gel method: (a) Ag-doped TiO<sub>2</sub> and (b) Ag-doped TiO<sub>2</sub>/PVA.

**Şekil 4.** Sol-jel yöntemi ile sentezlenen nanokompozit tozların UV-vis pik değerleri: (a) Ag katkılı TiO<sub>2</sub> ve (b) Ag katkılı TiO<sub>2</sub>/PVA.

**Table 4.** The band gap values ( $E_g$ ) of pure, Ag-doped TiO<sub>2</sub> and TiO<sub>2</sub>/PVA nanocomposite powders.

**Tablo 4.** Saf, Ag katkılı TiO<sub>2</sub> ve TiO<sub>2</sub>/PVA nanokompozit tozların bant aralığı değerleri ( $E_g$ ).

Sample code	Band gap ( $E_g$ , eV)
T	3.34
T-2A	3.27
T-2A3P	3.26
T-4A	3.18
T-4A3P	3.17

### 3.3. Antibacterial properties of nanocomposite powders

#### 3.3. Nanokompozit tozların antibakteriyel özellikleri

Antibacterial behaviors of the synthesized pure, Ag-doped TiO<sub>2</sub> and TiO<sub>2</sub>/PVA nanocomposite powders were valued by Gram-negative and Gram-positive bacterias in our study. The most preferred *S. aureus* and *E. coli* strains, causing hospital infections, were used during the tests (Aydin et al., 2014). TiO<sub>2</sub>, Ag-doped TiO<sub>2</sub> (T-2A and T-4A), and Ag-doped TiO<sub>2</sub>/PVA (T-2A3P and T-4A3P) nanocomposite powders were challenged with high *E. coli* and *S. aureus* bacteria levels (at concentrations of around 10<sup>5</sup> CFU/mL). The bacterial reduction results are given in Figure 5.

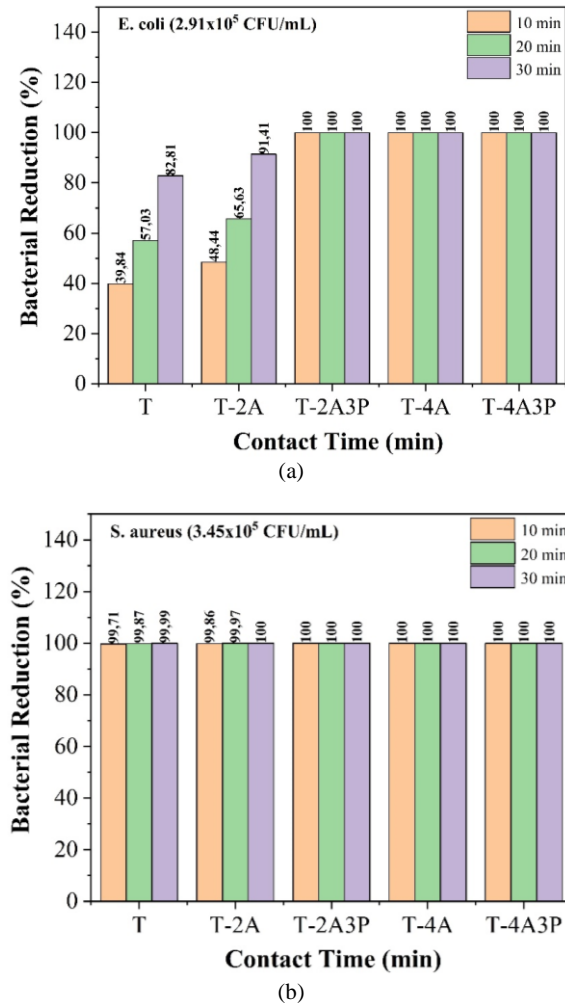


**Figure 5.** Antibacterial properties of the synthesized nanocomposite powders: (a) Gram-negative bacterium *E. coli* and (b) Gram-positive bacterium *S. aureus*.

**Şekil 5.** Sentezlenen nanokompozit tozların antibakteriyel özellikleri: (a) Gram negatif bakteri *E. coli* ve (b) Gram pozitif bakteri *S. aureus*.

While the undoped control nanopowders (T) exhibit less antibacterial property in both tests, Ag-doped TiO<sub>2</sub> and TiO<sub>2</sub>/PVA deactivated all bacteria (100%) throughout the tests within the contact times of 10 minutes, 20 minutes, and 30 minutes. T, T-2A, T-2A3P, T-4A, and T-4A3P provided deactivation of 99.99%, 100%, 100%, 100%, and 100% (respectively) within 30 minutes when challenged with *S. aureus* and provided deactivation of 82.81%, 91.41%, 100%, 100%, and 100% (respectively) within 30 minutes when challenged with *E. coli*. The deactivation performance of the Ag-doped TiO<sub>2</sub> and TiO<sub>2</sub>/PVA nanocomposite powders to Gram-negative bacteria is lower than Gram-positive bacteria due to the nanocomposite powders of Gram-negative strains. An increasing amount of Ag concentration improved the antibacterial behavior of the

synthesized Ag-doped TiO<sub>2</sub> and TiO<sub>2</sub>/PVA nanocomposite powders. Ag nanoparticle is used such as antibactericidal agent due to carrying antibacterial property and enhances the antibacterial effect for a variety of applications (Panacek et al., 2006). Since Ag nanoparticles have been proved as a potential antibacterial agent, the possible mode of increase in antibacterial effect of Ag doped TiO<sub>2</sub>/PVA nanocomposite powders may be due to release of Ag nanoparticles from the TiO<sub>2</sub>/PVA matrix (Cha et al., 2012; Swaroop et al., 2016).

## 4. Conclusions

### 4. Sonuçlar

Pure, Ag-doped TiO<sub>2</sub> and TiO<sub>2</sub>/PVA nanocomposite powders were successfully prepared in the form of homogeneous spherical morphologies by the sol-gel method. This method can be applied to all-ceramic systems to produce high-density materials. It is proven that polymeric binders like PVA are essential for spherical morphology with this study. The X-ray diffraction analysis of TiO<sub>2</sub> based composite powders confirms the formation of tetragonal structure and not the emergence of another secondary phase. The decrease in the surface area of TiO<sub>2</sub> particles synthesized by the sol-gel method was observed due to spherical morphology. Elemental analysis results revealed the presence of Ag in the composite powders synthesized by the sol-gel method. Ag-doped TiO<sub>2</sub> and TiO<sub>2</sub>/PVA nanocomposite powders showed optical properties, which can be demanded by different engineering needs. The Ag-doped TiO<sub>2</sub> and TiO<sub>2</sub>/PVA nanocomposite powders ensured significant deactivation against *E. coli* and *S. aureus* of about 10<sup>5</sup> CFU within 10 minutes, 20 minutes, and 30 minutes of contact times. The pure nanopowders show less antibacterial behavior.

## Acknowledgment

*Teşekkür / Katkı belirtme*

The authors are grateful to Inst. Murat EROĞLU for his support in the morphological characterization. The authors would like to thank the Central Research Laboratory at Bursa Technical University for the SEM/EDS analyses.

## Author contribution

*Yazar katkısı*

Concept/Design: ŞD, BB; Data Collection and/or Processing: ŞD, BB; Data analysis and interpretation: ŞD, BB; Literature Search: ŞD, BB;

Drafting manuscript: ŞD, BB; Critical revision of manuscript: ŞD, BB

### Declaration of ethical code

*Etik beyanı*

The authors declare that all of the rules stated to be followed within the scope of the “Higher Education Institutions Scientific Research and Publication Ethics Directive” were followed, and none of the actions specified under the title of “Actions Contrary to Scientific Research and Publication Ethics” have been taken.

### Conflicts of interest

*Çıkar çatışması beyanı*

The authors declare that they have no conflict of interest.

### References

*Kaynaklar*

- Abbad, S., Guergouri, K., Gazaout, S., Djebabra, S., Zertal, A., Barille, R., & Zaabat, M. (2020). Effect of silver doping on the photocatalytic activity of TiO<sub>2</sub> nanopowders synthesized by the sol-gel route. *Journal of Environmental Chemical Engineering*, 8(3), 103718. <https://doi.org/10.1016/j.jece.2020.103718>
- Aksu, A., Taskin, Ö, S., Cetintasoglu, M, E., Korkmaz, N, E., Torlak, C., & Caglar, N. (2020). Preparation of silica based C8 packing material from non-toxic water glass. *International Journal of Environment and Geoinformatics*, 7(2), 127-131. <https://doi.org/10.30897/ijegeo.700599>
- Ali, T., Ahmed, A., Alam, U., Uddin, I., Tripathi, P., & Muneer, M. (2018). Enhanced photocatalytic and antibacterial activities of Ag-doped TiO<sub>2</sub> nanoparticles under visible light. *Materials Chemistry and Physics*, 212, 325-335. <https://doi.org/10.1016/j.matchemphys.2018.03.052>
- Bahadur, J., Agrawalet, S., Panwar, V., & Parveen, A. (2016). Antibacterial properties of silver doped TiO<sub>2</sub> nanoparticles synthesized via sol-gel technique. *Macromolecular Research*, 24(6):488–493. <https://doi.org/10.1007/s13233-016-4066-9>
- Bandyopadhyay, A., Sarkar, M., & Bhowmick, A. K. (2005). Poly(vinyl alcohol)/silica hybrid nanocomposites by sol-gel technique: synthesis and properties. *Journal of Materials Science*, 40(19), 5233-5241. <https://doi.org/10.1007/s10853-005-4417-y>
- Behnajady, M. A., Modirshahla, N., Shokri, M., & Rad, B. (2008). Enhancement of photocatalytic activity of TiO<sub>2</sub> nanoparticles by silver doping: photodeposition versus liquid impregnation methods. *Global Nest Journal*, 10(1), 1–7. <https://doi.org/10.30955/gnj.000485>
- Brinker, C. J., Frye, G. C., Hurd, A. J., & Ashley, C. S. (1991). Fundamentals of sol-gel dip coating. *Thin Solid Films*, 201(1), 97-108. [https://doi.org/10.1016/0040-6090\(91\)90158-T](https://doi.org/10.1016/0040-6090(91)90158-T)
- Bulut, B., & Duman, Ş. (2021). Effects of calcination temperature on hydrothermally synthesized titanium dioxide submicron powders. *Konya Journal of Engineering Sciences*, 9(3), 676-685. <https://doi.org/10.36306/konjes.915062>
- Cha, H. R., Babu, V. R., Rao, K. S. V. K., Kim, Y. H., Mei, S. R., Joo, W. H., & Lee, Y. (2012). Fabrication of amino acid based silver nanocomposite hydrogels from PVA- poly(acrylamide-co-acryloyl phenylalanine) and their antimicrobial studies. *Bulletin of the Korean Chemical Society*, 33(10), 3191-3195.
- Chandra, A., Turng, L. S., Gopalan, P., Rowell, R. M., & Gong, S. (2008). Study of utilizing thin polymer surface coating on the nanoparticles for melt compounding of polycarbonate/alumina nanocomposites and their optical properties. *Composites Science and Technology*, 68, 768–776. <https://doi.org/10.1016/j.compscitech.2007.08.027>
- Chang, J. H., An, Y. U., Cho, D., & Giannelis, E. P. (2003). Poly(lactic acid) nanocomposites: comparison of their properties with montmorillonite and synthetic mica (II). *Polymer*, 44, 3715–3720. [https://doi.org/10.1016/S0032-3861\(03\)00276-3](https://doi.org/10.1016/S0032-3861(03)00276-3)
- Chao, H. E., Yun, Y. U., Xingfang, H. U., & Larbot, A. (2003). Effect of silver doping on the phase transformation and grain growth of sol-gel titania powder. *Journal of the European Ceramic Society*, 23(9), 1457–1464. [https://doi.org/10.1016/S0955-2219\(02\)00356-4](https://doi.org/10.1016/S0955-2219(02)00356-4)
- Cheng, Q., Li, C., Pavlineket, V., Saha, P., & Wang, H. (2006). Surface-modified antibacterial TiO<sub>2</sub>/Ag<sup>+</sup> nanoparticles: Preparation and properties. *Applied Surface Science*, 252(12), 4154–4160. <https://doi.org/10.1016/j.apsusc.2005.06.022>
- Crispim, E. G, Piai, J. F., Fajardo, A. R., & Ramos, E. R. F., Nakamura, T. U., Nakamura, C. V., Rubira, A. F., Muniz, E. C. (2012). Hydrogels based on chemically modified poly(vinyl alcohol) (PVA-GMA) and PVA-GMA/chondroitin sulfate: Preparation and characterization. *Express Polymer Letters*, 6, 383-395.

- <https://doi.org/10.3144/expresspolymlett.2012.41>
- Fang, H., Wang, J., Li, L., Xu, L., Wu, Y., Wang, Y., Fei, X., Tian, J., & Li, Y. (2019). A novel high-strength poly(ionic liquid)/PVA hydrogel dressing for antibacterial applications. *Chemical Engineering Journal*, 365, 153-164. <https://doi.org/10.1016/j.cej.2019.02.030>
- Feng, O. L., Wu, J., Chen, G. Q., Cui, F. Z., Kim, T. N., & Kim, J. O. (2000). A mechanistic study of the antibacterial effect of silver ions on *Escherichia coli* and *Staphylococcus aureus*. *Journal of Biomedical Materials Research*, 52(4), 662-668. [https://doi.org/10.1002/1097-4636\(20001215\)52:4<662:aid-jbm10>3.0.co;2-3](https://doi.org/10.1002/1097-4636(20001215)52:4<662:aid-jbm10>3.0.co;2-3)
- Feng, W., Mu-Sen, L., Yu-Peng, L., & Yong-Xin, Q. (2005). A simple sol-gel technique for preparing hydroxyapatite nanopowders. *Materials Letters*, 59(8-9), 916-919. <https://doi.org/10.1016/j.matlet.2004.08.041>
- Francis, S., Kumar, M., & Varshney, L. (2004). Radiation synthesis of superabsorbent poly(acrylic acid)-carrageenan hydrogels. *Radiation Physics and Chemistry*, 69(6), 481-486. <https://doi.org/10.1016/j.radphyschem.2003.09.004>
- Duman, Ş., & Özkal, B. (2012). Effect of initial powder properties on the granulation behavior of PVA added ZnO powders. *16<sup>th</sup> International Metallurgical & Materials Congress (IMMC 2012)* (ss. 182-189). İstanbul.
- Haque, F. Z., Nandanwar, R., & Singh, P. (2017). Evaluating photodegradation properties of anatase and rutile TiO<sub>2</sub> nanoparticles for organic compounds. *Optik*, 128, 191-200. <https://doi.org/10.1016/j.ijleo.2016.10.025>
- Han, K., & Yu, M. (2006). Study of the preparation and properties of UV-blocking fabrics of a PET/TiO<sub>2</sub> nanocomposite prepared by in situ polycondensation. *Journal of Applied Polymer Science*, 100, 1588-1593. <https://doi.org/10.1002/app.23312>
- Holzwarth, U., & Gibson, N. (2011). The scherrer equation versus the 'debye-scherrer equation'. *Nature Nanotechnology*, 6, 534-534. <https://doi.org/10.1002/app.23312>
- Guo, Z., Pereira, T., Choi, O., Wang, Y., & Hahn, H.T. (2006). Surface functionalized alumina nanoparticle filled polymeric nanocomposites with enhanced mechanical properties. *Journal of Materials Chemistry*, 16, 2800-2808. <https://doi.org/10.1039/B603020C>
- Jamuna-Thevi, K., Bakar, S. A., Ibrahim, S., & Shahab, N. (2011). Quantification of silver ion release, in vitro cytotoxicity and antibacterial properties of nanostructured Ag doped TiO<sub>2</sub> coatings on stainless steel deposited by RF magnetron sputtering. *Vacuum*, 86(3), 235-241. <https://doi.org/10.1016/j.vacuum.2011.06.011>
- Jr Walker, W. J., Reed, J. S., & Verma, S. K. (1999). Influence of slurry parameters on the characteristics of spray-dried granules. *Journal of the American Ceramic Society*, 82(7), 1711-1719. <https://doi.org/10.1111/j.1151-2916.1999.tb01990.x>
- Kawashita, M., Tsuneyama, S., Miyaji, F., Kokubo, T., Kozuka, H., & Yamamoto, K. (2000). Antibacterial silver-containing silica glass prepared by sol-gel method. *Biomaterials*, 21(4), 393-398. [https://doi.org/10.1016/S0142-9612\(99\)00201-X](https://doi.org/10.1016/S0142-9612(99)00201-X)
- Lee, K., Guan, B. H., Zaid, H. M., Soleimani, H., & Ching D. L. C. (2016) Impact of pH on zinc oxide particle size by using sol-gel process. *4<sup>th</sup> International Conference on Fundamental and Applied Sciences (ICFAS 2016)* (pp. 1787), Kuala Lumpur, Malaysia. <https://doi.org/10.1063/1.4968109>
- Lei, X. F., Xue, X. X., & Yang, H. (2014). Preparation and characterization of Ag-doped TiO<sub>2</sub> nanomaterials and their photocatalytic reduction of Cr (VI) under visible light. *Applied Surface Science*, 321, 396-403. <https://doi.org/10.1016/j.apsusc.2014.10.045>
- Liu, C., & Shaw, L. (2015). Nanoparticulate materials and core/shell structures derived from wet chemistry methods. In B. Bhushan (Eds.), *Encyclopedia of Nanotechnology* (ss. 1-21). Dordrecht: Springer Netherlands. [https://doi.org/10.1007/978-94-017-9780-1\\_100906](https://doi.org/10.1007/978-94-017-9780-1_100906)
- Livage, J., Henry, M., & Sanchez, C. (1988). Sol-gel chemistry of transition metal oxides. *Progress in Solid State Chemistry*, 18, 259-341. [https://doi.org/10.1016/0079-6786\(88\)90005-2](https://doi.org/10.1016/0079-6786(88)90005-2)
- Li, J., Xie, B., Xia, K., Li, Y., Han, J., & Zhao, C. (2018). Enhanced antibacterial activity of silver doped titanium dioxide-chitosan composites under visible light. *Materials*, 11(8), 1403. <https://doi.org/10.3390/ma11081403>
- Mathews, N. R., Morales, E. R., Cortés-Jacome, M. A., & Antonio, J. T. (2009). TiO<sub>2</sub> thin films—Influence of annealing temperature on structural, optical and photocatalytic properties. *Solar Energy*, 83(9), 1499-1508. <https://doi.org/10.1016/j.solener.2009.04.008>

- Mogal, S. I., Gandhi, V. G., Mishra, M., Tripathi, S., Shripathi, T., Joshi, P. A., & Shah, D. O. (2014). Single-step synthesis of silver-doped titanium dioxide: influence of silver on structural, textural, and photocatalytic properties. *Industrial & Engineering Chemistry Research*, *53*(14), 5749–5758. <https://doi.org/10.1021/ie404230q>
- Shenhar, R., Norsten, T.B., & Rotello, V.M. (2005). Polymer-mediated nanoparticle assembly: structural control and applications. *Advanced Materials*, *17*, 657–669. <https://doi.org/10.1002/adma.200401291>
- Seery, M. K., George, R., Floris, P., & Pillai, S. C. (2007). Silver doped titanium dioxide nanomaterials for enhanced visible light photocatalysis. *Journal of Photochemistry and Photobiology A: Chemistry*, *189*(2-3), 258–263. <https://doi.org/10.1016/j.jphotochem.2007.02.010>
- Sun, S. -Q., Sun, B., Zhang, W., & Wang, W. (2008). Preparation and antibacterial activity of Ag-TiO<sub>2</sub> composite film by liquid phase deposition (LPD) method. *Bulletin of Materials Science*, *31*(1), 61–66. <https://doi.org/10.1007/s12034-008-0011-7>
- Swaroop, K., Francis, S., & Somashekarappa, H. M. (2016). Gamma irradiation synthesis of Ag/PVA hydrogels and its antibacterial activity. *Materials Today: Proceedings*, *3*, 1792–1798. <https://doi.org/10.1016/j.matpr.2016.04.076>
- Varshney, L. (2007). Role of natural polysaccharides in radiation formation of PVA – hydrogel wound dressing. *Nuclear Instruments and Methods in Physics Research, Section B: Beam Interactions with Materials and Atoms*, *255*, 343–349. <https://doi.org/10.1016/j.nimb.2006.11.101>
- Viet, P. V., Phan, B. T., Mott, D., Maenosono, S., Sang, T. T., Thi, C. M., & Hieu, L. V. (2018). Silver nanoparticle loaded TiO<sub>2</sub> nanotubes with high photocatalytic and antibacterial activity synthesized by photoreduction method. *Journal of Photochemistry and Photobiology A: Chemistry*, *352*, 106–112. <https://doi.org/10.1016/j.jphotochem.2017.10.051>
- Wang, G., (2007). Hydrothermal synthesis and photocatalytic activity of nanocrystalline TiO<sub>2</sub> powders in ethanol-water mixed solutions. *Journal of Molecular Catalysis A: Chemical*, *274*, 185–191. <https://doi.org/10.1016/j.molcata.2007.05.009>
- Wang, Y., Cheng, H., Hao, Y., Ma, J., Li, W., & Cai, S. (1999). Preparation, characterization and photoelectrochemical behaviors of Fe (III)-doped TiO<sub>2</sub> nanoparticles. *Journal of Materials Science*, *34*(15), 3721–3729. <https://doi.org/10.1023/A:1004611724069>
- Williamson, G. K., & Hall, W. H. (1953). X-ray line broadening from fcc aluminium and wolfram. *Acta metallurgica*, *1*(1), 22–31. [https://doi.org/10.1016/0001-6160\(53\)90006-6](https://doi.org/10.1016/0001-6160(53)90006-6)
- Wu, T., & Ke, Y. (2007). Melting, crystallization and optical behaviors of poly (ethylene terephthalate)-silica/polystyrene nanocomposite films. *Thin Solid Films*, *515*, 5220–5226. <https://doi.org/10.1016/j.tsf.2006.12.029>
- Ye, C. Q. (2018). Sol-gel processes of functional powders and films, In C. Saravanan (Eds.), *Chemical reactions in inorganic chemistry*, (ss. 31-50). InTech: London, UK. <https://doi.org/10.5772/intechopen.69588>
- Yildirim, S. (2021). Synthesis, characterization and optical properties of Ag-doped TiO<sub>2</sub> nanoparticles by flame spray pyrolysis. *Journal of Materials Science: Materials in Electronics*, *32*, 16346–16358. <https://doi.org/10.1007/s10854-021-06187-9>
- Yin, S., Zhang, Q., Saito, F., & Sato, T., (2003). Preparation of visible light-activated titania photocatalyst by mechanochemical method. *Chemistry Letters*, *32*, 358–359. <https://doi.org/10.1246/cl.2003.358>
- Zhang, Z., Wan, M., & Mao, Y. (2012). Enhanced photovoltaic effect of TiO<sub>2</sub>-based composite ZnFe<sub>2</sub>O<sub>4</sub>/TiO<sub>2</sub>. *Journal of Photochemistry and Photobiology A: Chemistry*, *233*, 15–19. <https://doi.org/10.1016/j.jphotochem.2012.02.009>